Siri Kolle Kleivane
Bernt Johan Leira
Sverre Steen

http://dx.doi.org/10.21278/brod74106

ISSN 0007-215X
eISSN 1845-5859

Development of a reliability model for crack growth occurrence for a secondary hull component

UDC 539.421:536.911:621.43:629.5.018.4
Original scientific paper

Summary

Ship hull vibration is a major contributor to fatigue crack growth and main engine excitation is identified as an important vibration source. A general method to solve any vibration problem arising onboard a ship does not exist, which encourages the use of a reliability-based framework for assessing ship vibration and its consequences. A stochastic model of vibration response is developed for the probabilistic formulation of the failure probability of the occurrence of crack propagation of a secondary structural hull component. The secondary structural component considered is a pipe stack support. The pipe stack support connects a cargo pump pipe stack to the wall inside the cargo tank, and the support is welded directly onto this wall. First, a generic cargo hold model is analysed with engine speed and the relative distance between the engine and the structural component under consideration as stochastic variables. Then, submodels are used to investigate the local vibration of the support and the stress response is evaluated for a combination of different engine speeds and relative distances. A surface is fitted to the vibration response and used for probabilistic analysis by Monte Carlo (MC/DSPS) and FORM/SORM reliability methods. The limit state is formulated as the possibility of fatigue crack growth based on a threshold stress intensity factor. This threshold factor depends on the initial crack size and different initial sizes are investigated. The adequacy of the functional representation for the stochastic model, which is fitted to discrete data points, is also assessed. It is seen that a functional representation using a sum of sine terms give an adequate fit for describing the stress response induced by engine speed, while a polynomial representation was adequate for the relative distance variable. The failure probability estimated by Monte Carlo simulations and SORM indicates that the pipe stack support is not critical for the occurrence of fatigue crack growth. A main observation from the analysis is that the reliability-based design of secondary structural components, also looking at the interaction with the global structure, may help to improve the vibration-induced stresses in local hull details by application of proper design measures.

Key words*:* *Fatigue crack growth; FORM/SORM; main engine excitation; Monte Carlo simulation; structural reliability analysis*

1. Introduction

This work introduces preliminary reliability analysis concerning vibration leading to fatigue of secondary structural components attached to the internal wall of a tanker hull. A secondary component is presently considered to be a supporting component of a larger structural set or system, which function may for instance be to provide stiffness or connect equipment or sub-structures to a larger structure or system, such as connecting a cargo pump to the inner side plating of the cargo tank. The primary function of the pipe stack support is to attach the cargo pump pipe stack to the tank wall, and it is welded directly to the tank wall during installation of the cargo pump at the shipyard. This is investigated by looking at global and local vibration and their interaction. Over time, significant vibration may lead to the malfunction of machinery or equipment and may cause fatigue failure of local structural components. Welded components are particularly susceptible to fatigue failure due to the welding procedure and presence of the weld itself. Fatigue failure accounts for around 80% of all mechanical engineering failures of marine structures worldwide, and ship hull vibration is a major contributor to fatigue crack growth [1]. Fatigue failure of a pipe stack support may lead to malfunction of the pumping process or damage to the pipes which in a worst-case scenario can prevent the operability of the cargo tank. Therefore, it is important to assess vibration characteristics and fatigue occurrence for such secondary components.

The primary sources of hull vibration are the main engine, the propeller as well as hydrodynamic loading (slamming and whipping). A substantial number of studies have primarily focused on hull vibration at a global scale (e.g., [2]; [3]; [4]). More recently, Samad et al. (2021) investigated the slamming impact on small high-speed passenger crafts. Severe slamming of such vessels may pose a danger to passengers' safety and health [5]. In addition, severe slamming introduces significant hull girder vibration. This may result in high-frequency cyclic oscillations of the hull girder which is a contributor to fatigue damage. Another example, and a vibration aspect which is becoming increasingly important, is the investigations of vessels in polar regions. van Zijl et al. (2021) used operational modal analysis to identify structural modes using vibration responses measured under normal operating conditions from wind, waves, and sea-ice excitations [6]. These studies relate to vibration at a global scale, and the interaction of global and local structural vibration and how this may affect local details, such as stringers and supports, has not been studied to the same extent. Leheta et al. (2016) investigated fatigue crack growth in ship structural details considering loads from varying sea water pressure on the outer shell of the hull structure [7]. More recently, Zhao et al. (2021) introduces a reliability approach to fatigue crack propagation analysis of ship structures in polar regions, where they investigate fatigue due to ice loads [8].

In ship design, when ensuring that the vessel will not be subjected to excessive levels of vibration, it is aimed to avoid resonance. Such assessments need to be based on both structural considerations and effects on human comfort and working conditions. Resonance occurs when the natural vibrations of a ship or a superstructure coincide with the excitation frequencies within the operating speed range of the vessel [9]. However, because of the many modes of vibration within the ship response, it is almost impossible to avoid the occurrence of resonance. The many different modes of vibration are due to the ship taking on different natural modes by diverse loading conditions, and the propulsion plants will operate at variable speeds leading to variable excitation frequencies [10]. The objective then becomes to avoid excessive resonance. Classification societies play a key role in defining the most suitable approaches to deal with vibration analysis of ship structures. These societies recommend practices, standards, and guidelines for vibration analysis and vibration limits, usually oriented towards a structural capacity assessment of the ship on an operational basis [10][11]. Vibration calculations of a ship structure are challenging due to the complexity by which the vibration response is governed

at both global and local levels. The influence of several parameters describing the physics of the vibration phenomena must be carefully considered, however, many of these are often only known at an approximate level. Accordingly, a general method to solve any kind of vibration problem arising onboard a ship does not exist [12]. Each problem must be assessed under the given circumstances, such as operational conditions, environmental loading, and characteristics of machinery and propulsion systems. This encourages the use of a reliability-based framework for assessing ship vibration and its consequence.

Over the decades, new vibration aspects have occurred due to changes in ship design and ship operation requirements. For instance, low-cost building such as light weight construction influences the values of stiffness and mass, and the use of fuel-efficient slow-running main engines for speed reduction and ship energy efficiency have altered the vibration picture onboard ships. Moreover, the demand for higher living comfort and consistent application of labour legislation rules underlined the need to reduce vibration levels. Much research has been dedicated to investigating these aspects, especially since the International Maritime Organization introduced their Energy Efficiency Design Index in 2011. More recently, Kalajdžić et al. (2022) investigated the energy efficiency of already existing ships where the only main particular that can be optimized in a meaningful way is the required engine power, and thus the speed. To meet an energy efficient criterion, main engine power and speed reduction are necessary [13], so-called slow steaming. This may alter the vibration characteristics of the engine and introduce new vibration problems for a vessel that has already been in operation for several years. Main engine excitation is already identified as a primary source of vibration and the focus of this work will be on this excitation source.

2. Vibration excitations from marine diesel engines

The two-stroke low-speed marine diesel engine has been the reliable and preferred choice as the prime mover for ocean-going merchant vessels [14]. These types of engines are favoured because of their high efficiency and reliability, and their low cost compared to other propulsion machinery [14][15]. They operate in a speed range between 70 to 130 rpm (revolutions per minute), and there is usually a "direct drive" to the propeller shaft, meaning there is no requirement for reduction gear or speed reduction arrangement [16]. Correspondingly, this gives less complicated maintenance and servicing of the engine and driveline. The engine is normally bolted directly to the ship structure due to its invariably generous size and mass. This may lead to the engine vibration being fully transmitted to the engine’s base structure and propagating further onto the ship hull structure. Therefore, a major source of ship hull vibration is vibration excitation from the two-stroke low-speed engine, which may contribute to substantial levels of vibration in the ship hull structure [11][12].

The primary excitations of the engine are caused by the mass inertia forces and moments generated by the rotating and reciprocating actions, and the combustion pressure forces and moments. The engine will move and deform in a complicated pattern that is usually described by decomposing it into a set of basic vibration modes that are superimposed to describe the vibrating motion.

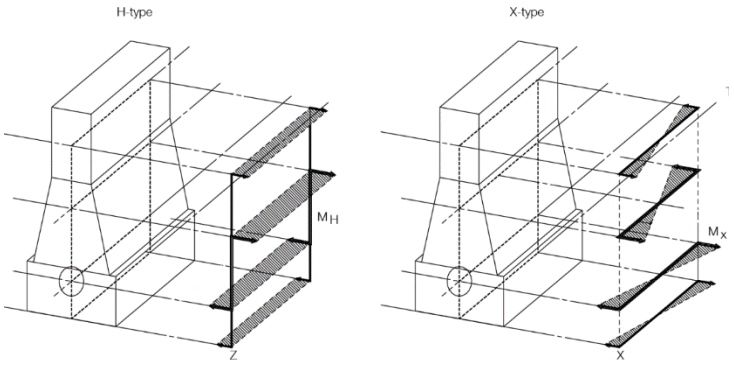

Fig. 1 Engine vibration modes [17]

The principal modes of vibration are the H-mode, causing a rocking behaviour of the engine, and the X-mode, causing a twisting of the engine, as seen in Figure 1. These excitations are called guide force moments and they result from the combustion process in the engine, which generates transverse reaction forces acting on the crosshead due to the connection rod/crankshaft mechanism. The guide force moments are usually harmless except when resonant vibration occurs in the engine/double bottom system [17], that is, in the dynamic interaction with the engine seating on the double bottom structure and resonant vibration occurs for the engine and the double bottom structure. Due to the accelerations of the rotating and oscillating parts, large unbalance inertia forces and moments are also generated and for engines with 5- or 6-cylinders, the most critical excitation is the external vertical 2nd order inertia moment [11][12]. These critical moments produce the most significant potential danger for severe hull vibrations. Therefore, ships with these types of main engines are usually equipped with moment compensators to mitigate critical vertical moments. A moment compensator may typically be an external electrically driven device that can neutralise the excitation when synchronised to the correct phase relive to the external moment [17].

2.1 Main engine model for vibration analysis

When the engine speed changes the order frequency, defined as the frequency times the order of the moment, of each moment will change and the magnitude of the moment will change. This is because the external forces and moments are influenced by engine speed, which gives oscillations of masses leading to unbalanced inertia effects, and by gas excitation which gives a cylinder pressure. Only guide force couples are considered as an excitation source since it can be assumed that a typical main engine in a tanker is installed with moment compensators. There are also mitigation measures possible for guide force excitation forces and moments. However, since they are usually of much smaller magnitude compared to the critical second-order moment, such mitigation measures are not often utilised. These forces will only be critical in the occurrence of resonance and the interest is thus to investigate possible resonance conditions, which may lead to excessive vibration even if the excitation forces are relatively small in magnitude.

Through contact with an engine manufacturer, data on external forces and moments for an engine typically used in medium or handysize tankers are provided. The engine is a 6-cylinder MAN B&W G50ME-C9.5, and the data is given for a power of 6875 kW achieved at 79 rpm and then for each engine rpm from 79 rpm until the engine speed reaches 90 rpm. This engine data has no connection to a particular real-life operation of a ship but is provided as a generic example for vibration simulation purposes. The data for the provided engine rating is given in Table 1 (not including orders with zero force).

Table 1 Data at a specific engine rating for a 6-cylinder MAN B&W G50ME-C9.5 typically used in in medium or handysize tanker.

Engine power of 6875 kW and engine speed of 79 r/min										
H- and X-mode guide force moment [kNm]										
Order	2. order	3. order	4. order	6. order	8. order	9. order	10. order	12. order	15. order	18. order
H-mode	-	-	-	825.5	-	-	-	65.7	-	20.6
X-mode	246.8	535.4	271.0	-	83.3	144.7	36.6	-	11.4	-

3. Structural reliability analysis and prediction

In a narrow sense, structural reliability is the probability that a structure will not attain each detailed limit state during a specified reference period [18]. Structural reliability assessments are thus concerned with the prediction of the probability of failure of a structural system at any stage during its lifetime. Failure is generally formulated as a limit state violation, $G(\boldsymbol{x}) \leq 0$, where G is an appropriate limit state function. The probability of the occurrence of an event such as a limit state violation is a numerical measure of the chance of its occurrence. Therefore, the failure probability may be used as a measure of safety, and it is a more explicit measure than the traditional use of safety factors [19].

Structural systems are both large and complex, and reliability calculations of such systems may involve multiple and often correlated states. The system loads and resistances may be dependent quantities and construction practices may influence member properties [19]. Simplifications and idealizations are often introduced to analyse these complex systems. Such simplifications may be concerning both the applied load and the response, the strength characteristics of the structural components, and the connection between the structural components and the system. Due to the introduction of modelling simplifications and idealizations, uncertainties are also introduced in the analysis. These uncertainties come in addition to the inherent uncertainties already present due to the random nature of the phenomena under consideration [18][19]. Thus, in all aspects of structural analysis and strength evaluation of marine structures, uncertainties are involved due to the randomness of geometric and material properties, the environment, and the inaccuracies in predictions of load, response, and strength [20].

The formulation of the reliability problem can be generalized in the following form:

$$p_f = P(G(\boldsymbol{x}) \leq 0) = \iint \dots \int_{G(\boldsymbol{x})\leq 0} f_x(\boldsymbol{x}) d\boldsymbol{x} \tag{1}$$

where p_f is the failure probability, $G(\boldsymbol{x}) < 0$ is the limit state formulation, and $f_X(\boldsymbol{x})$ is the joint probability density function (pdf) for the vector $\boldsymbol{x}$ of basic variables [18][20].

The integral in Eq. (1) cannot be solved analytically for general cases. However, this can still be possible for special cases, for instance, when the general formulation can be reduced to a one-dimensional integral. Numerical integration may be efficiently used; however, such methods are not used to a substantial extent in practice as they become inefficient for problems with many variables [18]. Approximation methods such as first-order and second-order reliability methods (FORM/SORM) are extensively used for the calculation of failure probability. The feasibility and accuracy of such methods are dependent on the non-linearity of the limit state function and the number of non-normal distributed variables [18][19]. A widely used alternative is determining the failure probability by Monte Carlo simulation, which in simple terms consists of sampling random points and checking whether each point is inside or outside of the defined event of interest [20].

3.1 FORM and SORM approximation methods

The first-order order reliability method (FORM) and the second-order reliability method (SORM) are developed as methods for approximation of the integral in equation (1). The basic idea for both methods is to transform the reliability problem from the given space of random variables, say $\boldsymbol{x}$, into a space of standard normal variables, denoted the $\boldsymbol{u}$-space. [18]. A general method for transforming dependent non-normal random variables into equivalent independent Gaussian distributed variables is the Rosenblatt transformation. With this transformation, the mapping from basic random variables to independent standard normal random variables preserves all statistical properties of the model. The Rosenblatt transformation for a single variable is illustrated in Figure 2, however, in general, this transformation needs to be done numerically.

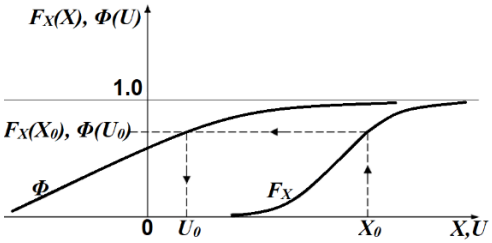

Fig. 2 Rosenblatt transformation for a single variable [21].

The main difference between the FORM and SORM is the order of the surface used for approximation of the surface of the boundary. The general principle of the FORM is to approximate the event boundary by linear surfaces at a selected set of points. The computational methods available for linear and piece-wise linear event boundaries are then applied to obtain an estimate of the event probability. The selection of linearisation points depends on the system configuration [22]. For a single event, the boundary is linearised at the design point $\boldsymbol{u}^*$, which is the point of maximum likelihood in the $\boldsymbol{u}$-space. A refinement of this method is introduced with the SORM, which approximates the boundary with a quadratic surface and an intersection of single events by a linear or parabolic surface [18][21]. For each case, the quadratic approximation is made at the design point $\boldsymbol{u}^*$. By using SORM, the class of problems that can be evaluated is significantly extended compared to FORM, as even highly curved failure domain boundaries can be well approximated. The basic concept of the two methods for approximating the failure probability is illustrated in Figure 3.

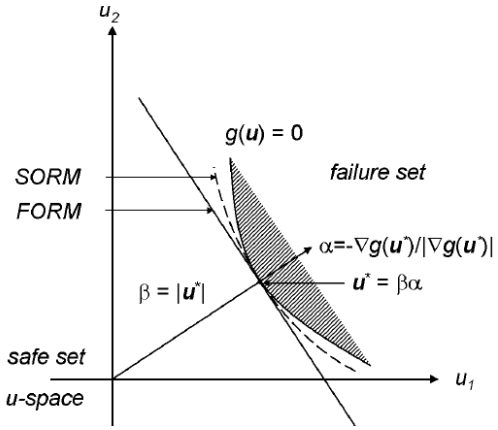

Fig. 3 Approximation to failure surface (FORM/SORM) [21]

3.2 Monte Carlo simulation methods

Monte Carlo simulation methods interpret probability as relative frequency [18] and involve simulating artificially many experiments by sampling at random and observing the results. A game of chance is by this approach constructed from known probabilistic properties to solve a problem many times and establish the failure probability from this [19]. The probability of the event is estimated as the average number of hits in the event during the simulation [22]. To use the Monte Carlo simulation technique in structural reliability assessments, the probability distribution of the stochastic variable must be estimated (chosen) and a systematic method for numerical sampling of the basic variables must be established [19]. The basic principle is illustrated in Figure 4.

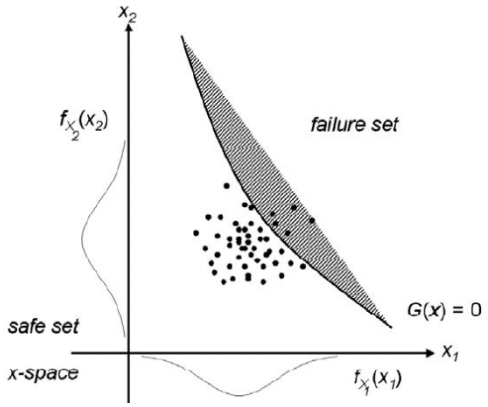

Fig. 4 Crude Monte Carlo simulation method [21].

There are different Monte Carlo simulation techniques. The simplest and possibly the most used approach is the 'crude' or direct Monte Carlo simulation, often called just Monte Carlo simulation, which is illustrated in Figure 4. However, this may not be the most efficient method and so-called variance reduction methods are often more cost-effective [18][19]. The direct method samples from a joint distribution of *n* stochastic basic variables, ***x*.** This is executed by first generating *n* uniformly distributed random variables and taking the inverse based on the distribution function of the stochastic variables. The failure probability is then expressed with an indicator function which gives the value 1 if a failure occurs and the value 0 otherwise:

$$p_f = \int \int_{all\ x} I\big(G(\boldsymbol{x})\big) f_{\boldsymbol{X}}(\boldsymbol{x}) d\boldsymbol{x} = E[I] \tag{2}$$

where *I()* is the indicator function given as:

$$I(G(\boldsymbol{x})) = \begin{cases} 1, & G(\boldsymbol{x}) \leq 0 \\ 0, & G(\boldsymbol{x}) > 0 \end{cases} \tag{3}$$

The failure probability is then estimated as:

$$\hat{p}_f = \frac{1}{N} \sum_{i=1}^{N} I\big(G(\hat{\boldsymbol{x}}_i)\big) = \frac{k}{N} \tag{4}$$

where the '^' indicates that it is an estimate, *k* is the number of failures (i.e., the number of times the limit state $G(\boldsymbol{x}) \leq 0$ is fulfilled), and *N* is the total number of sample simulations. To have a reasonable estimate for the failure probability, the number *N* of samples must be sufficient, and generally, a large sample size is required to obtain sufficiently accurate estimates.

The advantage of the crude Monte Carlo method is that it makes use of point values of the event function only. Thus, the event function is not required to be a smooth function of its

variables [19]. In addition, the estimate of the event probability is unbiased. Nevertheless, the direct simulation method has a severe computational penalty with a slow convergence (of the standard deviation), compared to traditional one-dimensional numerical integration, such as the trapezoidal rule and Simpson's rule. This penalty has led to so-called variance reduction techniques, which are essentially aimed at reducing the variance of the indicator function [18][19].

3.2.1 Importance sampling

Importance sampling is a Monte Carlo method combined with a variance reduction technique, also referred to as design point simulation in some literature [22]. In this method, known information about the problem is used to restrain the simulation to interesting regions [19]. This leads to far fewer samples required for a given level of confidence using importance sampling compared to the traditional crude Monte Carlo method. The basic idea is to concentrate the sampling around the area of the total sample space which has the largest contribution to the probability of failure [18]. This is done by finding the design point $\boldsymbol{u}^*$ and performing a Monte Carlo simulation by sampling around this point [22]. For each variable, the sampling density is a normal distribution centred at the design point. The process is demonstrated in Figure 5.

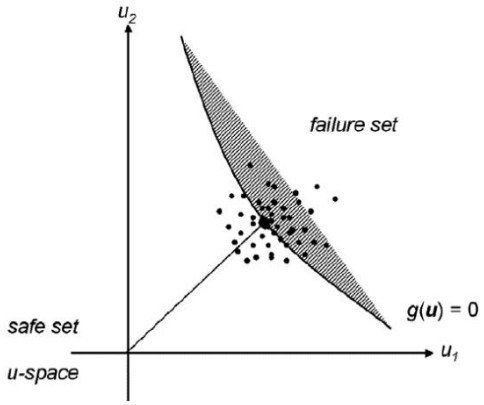

Fig. 5 Importance sampling [21].

As for the crude Monte Carlo method, the indicator function is also applied for the purpose of importance sampling. In addition, an importance-sampling pdf, $h_{\boldsymbol{X}}(\boldsymbol{x})$, is introduced. The modified expression for estimating the failure probability then becomes:

$$p_f = \int \dots \hat{p}_f = \frac{1}{N}\sum_{i=1}^{N} I(G(\hat{\boldsymbol{x}}_i))\frac{f_{\boldsymbol{X}}(\hat{\boldsymbol{x}}_i)}{h_{\boldsymbol{X}}(\hat{\boldsymbol{x}}_i)} \tag{5}$$

The importance-sampling pdf governs the distribution of the samples and the sample value vector, $\hat{\boldsymbol{x}}_i$, is in this case established from $h_{\boldsymbol{X}}(\boldsymbol{x})$. The goodness of the probability estimated will now depend on the choice of the importance-sampling pdf [18]. Ideally, this pdf is to be selected so that it lies in the region of most interest, which is the hyper-zone $G(\boldsymbol{x}) \leq 0$. However, this region is generally difficult to identify as there are no simple criteria with which to work [19]. The design point is utilised as an alternative to identifying the hyper-zone region and this point can for most pdfs be found by numerical maximization techniques, such as the FORM approximation technique. Therefore, in analysis tools, a FORM analysis is often first performed to identify the design point and then importance sampling Monte Carlo probability simulation is performed, with sampling density concentrated at the design point.

4. Methodology

4.1 Cargo hold model for vibration analysis

A finite element model of a generic cargo hold structure is analysed through harmonic vibration analysis where an acoustic module is utilised to consider the mass effect of the cargo. A cargo pump pipe stack is modelled in one of the mid-hold tanks, and the secondary structural hull component considered is a pipe stack support. To look at the response on a local level, submodels of the pipe stack and its supports are established. The sub-modelling technique is utilised to transfer the global response of the cargo hold model onto the submodel of the pipe stack and pipe stack supports. The generic cargo hold model consists of ½ + 1 + ½ cargo holds. The submodel consists of the pipe stack and its supports connected to a cut-out section of the tank wall. In addition, three smaller submodels, one of each of the pipe stack supports (top, middle, and bottom supports), are established to further evaluate hot spot stresses. The finite element models are shown in Figure 6 and Figure 7.

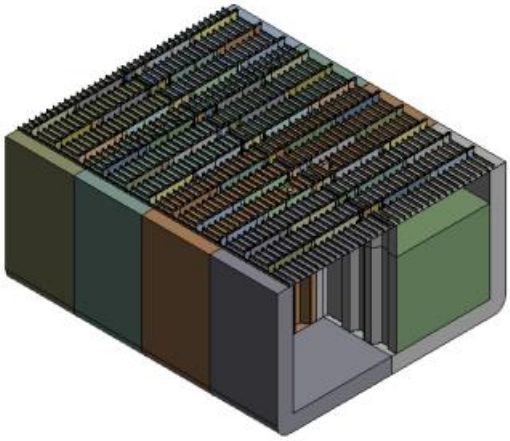

Fig. 6 Cargo hold model (75% filling level)

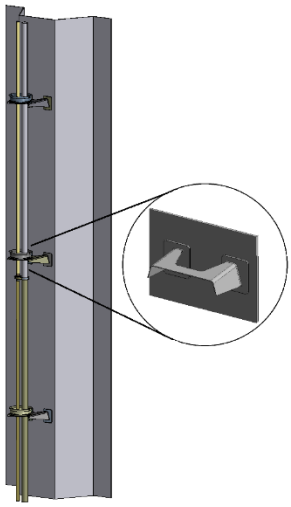

Fig. 7 Submodel of pipe stack and support

Natural frequencies of ship structures are typically in the range of 5-20 Hz [11][23], and through preliminary analyses, it is seen that the natural frequencies of the hold model, and the main engine, lie within this range. Accordingly, a specified frequency range from 0-20 Hz is used in the vibration analysis. The boundary conditions are implemented based on the recommendations given by DNV (2021) in their guideline for finite element analysis (DNV-CG-0127). They consist of rigid links applied at the model ends connected to an independent point and a point constraint to restrict unwanted rotation of the model, as seen in Figure 8. The sub-modelling technique is used for developing the submodels, where the nodal displacements of the global hold model are applied to the corresponding boundary nodes of the local model as prescribed displacement boundary conditions.

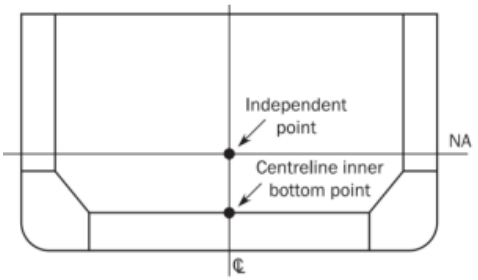

Fig. 8 Boundary conditions at model end sections [24].

The engine excitation loading is established as forces based on the engine's guide force moments and for modelling purposes, the size of the forces can be calculated as:

$$F = \frac{M}{L} \tag{6}$$

where F is the force, M is the guide force moment and L is the engine's connecting rod, i.e., the distance between the crankshaft level and the middle position of the crosshead guide. These forces will change for different engine speeds, and they are implemented in the analysis as remote forces acting on the aft end of the model. The combinations of six different engine speeds and six different relative distances between the location of the engine and the model's aft are analysed. Engine speed and relative distance are the stochastic variables chosen for the reliability model. This will be elaborated on later.

4.1.1 Distribution of cargo

The distribution of cargo along the length of the ship will directly influence the global hull bending and shearing stresses and stresses in the local hull structures. Through preliminary modal analysis respectively with empty cargo tanks as well as 25%, 50% and 75% filling levels, it is observed that when more volume is filled in the tanks, the lower the natural frequencies are, which is due to the increasing mass of the structure. It is also observed that for the case with a 75% filling level the highest number of natural frequencies coincided with engine excitation frequencies. Therefore, it is decided to use this scenario for further investigation, and a specific scenario with a 75% filling level in the tanks and an alternating loading configuration is analysed, as seen in Figure 9. Therefore, the presented cargo configuration is assumed to represent a case where the tank wall to which the cargo pump pipe stack is connected experiences large forces due to the additional mass of the cargo on the wall.

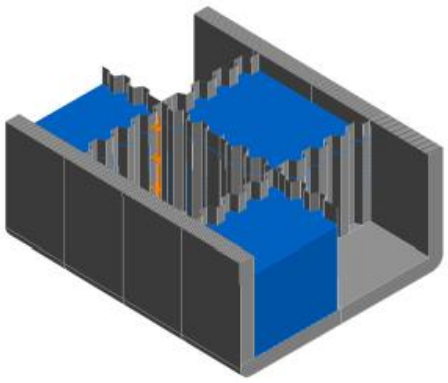

Fig. 9 Alternating load configuration

4.2 Probabilistic analysis

The probabilistic formulation of the problem is based on regression by fitting a surface to data points from the vibration analysis. When considering the occurrence of fatigue crack growth, crack propagation is usually assumed to occur in the vicinity of a hot spot, the location where large, concentrated stresses occur. The stress level is the driving source of crack propagation [25], therefore, the local stress on a pipe stack support is taken as the main response of interest. The engine speed (rpm) and the relative distance between the engine and the secondary component under consideration are selected as stochastic variables. They are both assumed to be described by uniform distributions.

The length of tanker hulls ranges from approximately 200m to 330m [26], and handysize or medium size tankers with an engine power as presented here are usually below the 200m

limit [27]. For an actual ship, the location of the engine will be fixed, however, by varying its placement relative to the mid-hold region, several ship sizes can be covered by the analysis. By this, how the size of the ship may influence the effect of engine excitation on the structural component can be investigated. The inherent assumption is then that the same type of engine is installed for the relevant range of ships with different hull sizes. Accordingly, the assumption of a uniform distribution can be argued as reasonable for the relative distance since different ship lengths are evaluated along the x-direction, then ranging from a minimum size to a maximum extent. These sizes are obtained based on assuming an initial size of 205m and then changing the size according to the typical ship lengths described above. However, the different sizes may not all comply with the power of the engine used in the analyses, but on the other hand, the range of sizes may also take into consideration differences in the location of the engine room and engine for different vessels. The assumption is more questionable for the engine speed. The engine's rpm will influence the magnitude of the forces and moments generated, and the operational speed of the engine will depend on the operating conditions and the ship's voyage. Therefore, it will most likely not have a uniform distribution. However, as a first step of the probabilistic analysis, and due to a lack of fleet information such as noon reports, a uniform distribution is assumed for both stochastic variables. The characteristics of these variables are given in Table 2.

Table 2 Stochastic variables

Stochastic variable	Definition	Distribution	Min – Max value	Standard deviation	Mean
X	Relative distance	Uniform	69-82 meter	3.8	75.5
Y	Engine speed	Uniform	79-120 rpm	11.8	99.5

The failure probability is estimated by Monte Carlo simulations using Proban, which is a general-purpose probabilistic analysis program developed by DNV [21] [22]. It can deal with a broad class of probabilistic and statistical problems encountered in engineering. Since Proban provides a variety of methods aimed at several types of probabilistic analysis, FORM and SORM analyses are also performed, to the extent that such methods produce feasible estimates. The results from the different methods are compared to evaluate the robustness of the calculations. A failure probability around 1 - 5% may be considered as not critical with regards to avoidance of possible fatigue cracking. However, due to a lack of information, it is at this stage difficult to establish an exact criterion for the acceptable probability of failure.

4.2.1 Surface fitting

The surface is established as the product of a functional representation for each of the stochastic variables. That is, one function is fitted to the engine speed and another to the relative distance, and assuming uncoupled parameter effects, the total response surface is the product of these two functions. Hereinafter, the stochastic variable 'relative distance' is referred to as *X* and the stochastic variable 'engine speed' is referred to as *Y*. The basic idea is to fit a surface to the inputs (x_i,y_i) and the outputs (z_i), where *Z* is the local stress response. Since *X* and *Y* are stochastic variables, the output *Z* will be a stochastic variable. The wanted functional representation will be on the form:

$$z(x,y) = g_L(x,y) = g_{L,X}(x) \cdot g_{L,Y}(y) \tag{7}$$

where g_L denotes the local stress response function to be investigated further in probabilistic analysis.

The integrity of fit may be evaluated by the following three statistical parameters: the sum of squares due to error (SSE), the R-square, and the root mean square error (RMSE). The SSE

expresses the total deviation of response values from the fit to the input response values, where a value close to zero indicates a fit more useful for prediction. The R-square parameter is a measure of how successful the fit is in explaining the variation of the data, and the closer to 1 the value is, the greater proportion of the variance is accounted for by the model. The RMSE gives an estimate of the standard deviation of the random component in the data, and a value closer to zero indicates a fit that is more useful for prediction [28].

4.2.2 Limit state for crack growth

The limit state is formulated as the possibility of fatigue crack growth. An estimate for the maximum allowable stress before crack propagation occurs is established based on the threshold stress intensity factor for crack growth of steel. The threshold stress intensity factor, ΔK_{th}, is taken as ΔK_{th} = 63MPa√mm [29]. The stress intensity factor range, ΔK is given as:

$$\Delta K = \Delta S\sqrt{\pi a}F(a) \tag{8}$$

where a is the instantaneous crack length, ΔS is the stress range, and $F(a)$ is the geometry function, which generally depends on the geometry of the body, the crack geometry and length, and the loading configuration. The limit value can then be formulated as:

$$S_{limit} = \frac{\Delta K_{th}}{\sqrt{\pi a}F} \tag{9}$$

For establishing maximum stress before crack propagation occurs, the geometry function is assumed to be equal to 1. Different initial crack sizes for welded structures are given in the literature, typically in the range of 0.1 – 0.5 mm [28][30]. A larger crack size will be more critical for the fatigue limit since it gives smaller allowable maximum stress, therefore, different initial crack sizes are evaluated to investigate what initial size may be critical for crack propagation for the secondary component under consideration. Table 3 gives different initial crack sizes and their corresponding maximum stress before crack propagation occurs.

Table 3 Initial crack sizes and fatigue limits

Initial crack size [mm]	S_{limit} [MPa]
0.1	112
0.3	64
0.5	50

The limit state function is now formulated as the possibility of the local stress of the structural component exceeding the established maximum allowable stress before crack propagation occurs:

$$G(\boldsymbol{x}) = S_{limit} - g_L \leq 0 \tag{10}$$

where the second term is defined by Eq. (6) above. Limit state violation will thus correspond to the occurrence of fatigue crack propagation.

5. Results of developed reliability model

5.1 Vibration analysis

The results from the harmonic vibration analysis are given in Table 4. The data points provide the stress response for the combination of each specific engine rpm and relative distance. The relative distance is given in meters, with the origin at the aft end of the model. The stress values are reported for the bottom support, at the hot spot seen in Figure 10.

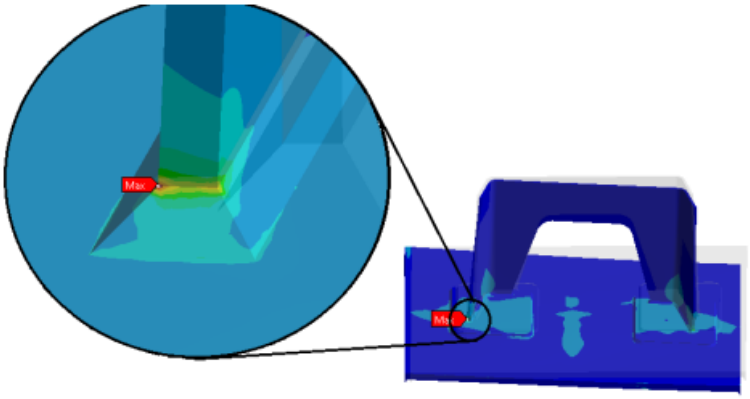

Fig. 10 Stress evaluation at bottom support.

Table 4 Data set of stress from vibration analysis, stress unit in MPa, distance in m.

RPM Relative distance	79	81	83	85	87	90
69	1.3924	1.6255	1.9623	2.8151	5.7185	5.9369
73	1.4922	1.8162	1.9287	2.8638	5.8724	5.7794
75	1.5269	1.7906	2.1646	2.9421	5.4232	6.3439
77	1.6058	1.8370	2.2850	3.0204	6.0799	6.5445
79	1.6054	1.7865	2.1810	3.0988	6.3924	6.3536
82	1.6207	1.9512	2.3321	3.3455	6.4644	7.2802

5.2 Fitted functions

The functional representations to best fit the stress data set for describing the stochastic variables are found to be 2nd order polynomial for the *X* variable (relative distance) and a sum of sine functions for the *Y* variable (engine speed). For both functional fits, the stress data is averaged over the relative range. That is, the *X* variable curve is evaluated at each coordinate for averaged stresses from the different rpms. The *Y* variable curve is evaluated at each rpm for averaged stresses from the different relative distances. The following equations are fitted to the data:

$$g_{L,X}(x) = a_1 \cdot x^2 + a_2 \cdot x + a_3 \tag{11}$$

$$g_{L,Y}(y) = b_1 \cdot \sin(b_2 y + b_3) + b_4 \cdot \sin(b_5 y + b_6) \tag{12}$$

The functional constants for each equation are given in Table 5 and the fitted curves are shown in Figure 11.

Table 5 Functional constants

Functional constants for X-variable			Functional constants for Y-variable					
a_1	a_2	a_3	b_1	b_2	b_3	b_4	b_5	b_6
3.0E-3	-0.406	16.99	21.39	0.360	-3.854	18.76	0.418	13.42

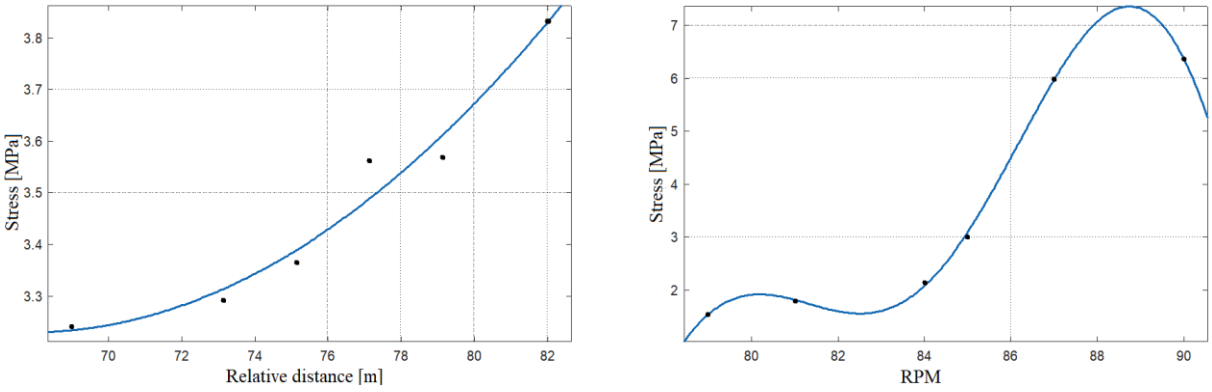

Fig. 11 Fitted functions based on stochastic variables *X* (left) and *Y* (right).

The goodness of fit statistics for the established functions are given in Table 6 and Table 7.

Table 6 Goodness of fit for X-variable

Parameter	SSE	R-square	RMSE
Value	0.0083	0.9660	0.0526

Table 7 Goodness of fit for Y-variable

Parameter	SSE	R-square	RMSE
Value	0.0103	0.9996	NaN

The SSE and R-square for both variables are satisfactory and no significant deviation of data points to the fitted curves is seen in either of the plots in Figure 11. The RMSE for the X variable is also satisfactory, however, for the Y variable the RMSE results in NaN (Not a Number), which means it may be dividing zero by zero or infinity. This is most likely related to what is called overfitting which means that the function is fitted too closely to a limited set of data points. Here there are only six data points for each fitted function which represents a relatively small data set. This error may be corrected by having a larger dataset on which to base the functional representation. However, consideration was made of the computational time required for each data point since the focus of the work is to investigate the functionality of the established reliability model for evaluating the occurrence of crack growth. It is also seen that the fit for the *X* variable may be somewhat badly conditioned due to the relatively small value for the constant a_1, which is something that may also be improved by having a larger vibration data sample.

The failure probability calculations are computed with the normalized versions of these response equations, to obtain the correct unit of the stress response (MPa). The variables are normalized based on the response value at relative distance of 77 m and engine speed of 85 rpm (see Table 4). This response value represents the reference value, and in the calculations, this is multiplied with the normalized values of the fitted response functions.

5.3 Failure probabilities

Table 8 summarises the computed failure probabilities obtained by application of the different methods, given as percentages. MC stands for Monte Carlo simulation and DSPS stands for design point simulation (importance sampling) The MC simulation is run with 500,000 random samples, and DSPS is run with 100,000 samples. These sample sizes are run in a matter of seconds, and they are deemed sufficient to obtain stable results.

Table 8 Failure probabilities

S_{max} [MPa]	MC	DSPS	FORM	SORM
50	2.21	2.23	24.15	1.08
55	0.28	0.26	10.16	0.35
60	~0	~0	~0	~0

The failure probabilities estimated for a fatigue limit stress of 60 MPa give values in the order of 10^{-2} percent and are thus evaluated as approximately equal to zero. The limit stress of 50 MPa corresponds to a crack size of 0.5 mm, and we see that for larger limit stress than 50 MPa, meaning smaller crack sizes than 0.5 mm, the estimated failure probabilities are quite small. However, it cannot be claimed based on this that the structure is safe since it is very difficult to establish failure criteria or target values for the analysis. It can only be concluded that fatigue crack growth at the pipe stack support has a quite low probability to occur.

The failure probabilities estimated by the two Monte Carlo simulation methods demonstrate the efficiency of the importance sampling compared to the Monte Carlo method. With a smaller sample size, the importance sampling method predicts the same failure probability as the Monte Carlo simulation, which here has five times the sample size. These failure probabilities also coincide relatively well with the failure probability estimated by the SORM formulation, compared to the FORM probability. The coincidence between MC, DSPS and SORM gives satisfying integrity associated with the calculation of failure probability. The failure probability estimated by the FORM gives different results than the other probability methods which may indicate that the failure surface (in normalized Gaussian space) is relatively curved and displays nonlinear characteristics. This agrees with the fact that the nonlinear approximation by SORM is more correct than the linear approximation by FORM, as compared to the Monte Carlo simulations. However, the estimated probabilities herein are obtained only based on the applied numerical methods and the associated calculation procedures They have not been compared with experimental data or measurements which must be kept in mind when discussing the integrity of the achieved results.

6. Conclusion

Satisfying integrity associated with the failure probability estimation is achieved and the validity of the result is supported by the relative coincidence between the probabilities estimated by means of SORM approximation, Monte Carlo simulation (MC), and importance sampling simulation (DSPS). Moreover, a first-order approximation is seen not to be suited for a feasible estimation of the failure probability. However, these results are only based on the comparison between the numerical methods used and no comparison to experimental data or measurements is made. The estimated failure probability for the largest initial crack size of 0.5 mm is below an acceptable limit for crack growth occurrence and the result indicates that the pipe stack support will not experience fatigue crack propagation. However, it cannot be concluded that the structure is safe in this regard, it can only be stated that it is quite unlikely to occur based on the current considerations. This is one of the criticisms of probabilistic methods, the target values are difficult to establish. It needs to be related to accurate descriptions of the loads and previous experience., including an assessment of the possible consequences of fatigue failure. If there is little previous experience, a target value of acceptable criteria is difficult to establish. This is also reflected by the influence of initial crack size, which largely affects the probability of the occurrence of crack propagation.

Although the failure probability estimation is relatively satisfactory, the assumption of a uniform distribution for engine speed is not a completely adequate representation of this

stochastic variable since the operational speed of the vessel depends on different parameters such as the voyage and environmental conditions. A better description of the distribution of the engine speed may be obtained by obtaining fleet information such as noon reports which report data such as the speed of the ship, environmental conditions, and the vessel positions daily. The uniform assumption of the relative distance is argued as reasonable since it is evaluated along the length of the ship. However, there might be an issue with overfitting the functional representation. This means that the model may only be useful for the initial data set on which it is based and may not be reliable for investigating the whole range of the stochastic variables. Therefore, for further development of the stochastic model, it may be preferable to have a larger data set for vibration response and to then cross-validate the model by investigating small portions of the data to average the overall error. A trade-off between sample size and the computational demand for the vibration analyses was made in this work since the aim was to evaluate the functionality of the reliability model, and then develop it further once it is deemed sufficient for the calculation of failure probabilities.

The resulting reliability model for assessing the possible occurrence of crack propagation for the pipe stack support demonstrates a potential for assessing the consequence of vibration response concerning fatigue crack growth. Based on the further development of this model for the different aspects described above and within the framework for reliability-based design of secondary structural components, this may serve as a helpful tool for improving the vibration characteristics of the local components, through structural optimization, and mitigating the risk of the occurrence of fatigue crack propagation.

REFERENCES

[1] Berge, S., Ås, S. K., 2017. Fatigue and Fracture Design of Marine Structures. *TMR4200 Compendium, third revised edition.*

[2] Jensen, J. Juncher, Dogliani. M., 1999. Wave-induced Ship Hull Vibrations in Stochastic Seaways. *Marine Structures*, 9.3-4, 353–387. https://doi.org/10.1016/0951-8339(95)00031-3

[3] Lee, S.-K., Liao, M., Wang, S. 2006. Propeller-induced hull vibration - analytical methods. *Proceedings of the 2nd International Ship Noise and Vibration Conference*, London, UK.

[4] Drummen, I., Storhaug, G., Moan, T., 2008. Experimental and numerical investigation of fatigue damage due to wave-induced vibrations in a containership in head seas. *Journal of Marine Science and Technology*, 13, 428–445. https://doi.org/10.1007/s00773-008-0006-5

[5] Abd Samad, F. I., Bin Mohd Yusop, M. Y., Bin Shaharuddin, N. M. R., Bin Ismail, N., Yaakob, O. B. 2021. Slamming impact accelerations analysis on small high speed passenger crafts. *Brodogradnja*, 72(1), 79–94. https://doi.org/10.21278/brod72104

[6] van Zijl, C., Soal, K., Volkmar, R., Govers, Y., Böswald, M., Bekker, A. 2021. The use of operational modal analysis and mode tracking for insight into polar vessel operations. *Marine Structures*, 79, 103043. https://doi.org/10.1016/j.marstruc.2021.103043

[7] Leheta, H., Elhewy, A., Younes, H., 2016. Analysis of Fatigue Crack Growth in Ship Structural Details. *Polish Maritime Research*, 23, 71-82. https://doi.org/10.1515/pomr-2016-0023

[8] Zhao, W., Leira, B. J., Feng, G., Gao, C., Cui, T., 2021. A reliability approach to fatigue crack propagation analysis of ship structures in polar regions. *Marine Structures*, 80, 103075. https://doi.org/10.1016/j.marstruc.2021.103075

[9] V. Ankudinov. Hydrodynamic Hull Damping (Phase I) 1991. Ship Structure Committee (SSC-359).

[10] Asmussen, I., Menzel, W., Mumm, H., 2001. GL Technology Ship Vibration. Germanischer Lloyd. Hamburg, Germany.

[11] American Bureau of Shipping (ABS), 2021. Guidance note on Ship Vibration. Texas, USA.

[12] Moro, L., Biot, M., Brocco, E., De Lorenxo, F., Vassallo, P. N. M., 2013. Hull vibration analysis of river boats. *International Conference IDS2013 – Amazonia*, Iquitos, Peru.

[13] Kalajdžić, M., Vasilev, M., Momčilović, N., 2022. Power reduction considerations for bulk carriers with respect to novel energy efficiency regulations. *Brodogradnja* 73(2), 79–92. https://doi.org/10.21278/brod73205

[14] MAN Energy Solutions. Two-Stroke Technology. 2021. https://marine.man-es.com/technology/low-speed-technology accessed 26th May 2022.

[15] Bukovac, Q., Medica, V., Mrzljak. V., 2015. Steady state performances analysis of modern marine two-stroke low speed diesel engine using mlp neural network model. *Brodogradnja* 66(4), 57–70.

[16] Anish Wankhede, A., 2021. Why 2-stroke Engines are Used More commonly than 4-stroke on Ships?, Marine Insight. https://www.marineinsight.com/main-engine/why-2-stroke-engines-are-used-more-commonly-than-4-stroke-on-ships/ accessed 28th December 2021.

[17] MAN Energy Solutions. MAN B&W G50ME-C9.6 Project Guide. 2022. url: https://man-es.com/applications/projectguides/2stroke/content/printed/G50ME-C9_6.pdf accessed 13th October 2022.

[18] Melchers, R. E., 1999. Structural reliability; analysis and prediction. *Wiley*, England.

[19] Bai, Y., Jin. W., 2016. Basics of Structural Reliability. In *Marine Structural Design*, second edition, *Butterworth-Heinemann*, Oxford, 581–602. https://doi.org/10.1016/B978-0-08-099997-5.00031-9

[20] Moan, T., 2009. Structural Risk and Reliability Analysis. Compendium. *Department of Marine Technology, NTNU*, Trondheim, Norway.

[21] Det Norske Veritas (DNV), 2014. SESAM User Manual Proban Theory. Det Norske Veritas, DNV Software Report No.: 96-7017. Høvik, Norway.

[22] Det Norske Veritas (DNV), 2004. SESAM User Manual Proban. Det Norske Veritas, DNV Software Report No.: 92-7049. Høvik, Norway.

[23] Lloyd's Register, 2015. Guidance Notes General Overview of Ship Structural Vibration Problems. *Lloyd's Register Group Limited*. United Kingdom, London.

[24] Det Norske Veritas (DNV), 2021. Class Guideline Finite element analysis. (DNV-CG-0127).

[25] Almar-Næss, A., 1985. Fatigue Handbook: offshore steel structures. *Tapir*, NTH - Norwegian University of Science and Technology, Trondheim, Norway.

[26] Notteboom, T., Pallis, A., Rodrigue, J., 2022. Port Economics, Management and Policy. London: Routledge, 2022. url: https://porteconomicsmanagement.org/pemp/contents/part8/ports-and-energy/tanker-size/ accessed 19th October 2022.

[27] MAN Energy Solutions, 2021. Propulsion trends in tankers. Denmark.

[28] MathWorks, Inc. Evaluating Goodness of Fit. 2021. url: https://se.mathworks.com/help/curvefit/evaluating-goodness-of-fit.html accessed 12th January 2021.

[29] British Standard, 2005. Guide to methods for assessing the acceptability of flaws in metallic structures. (BS 7910:2005), *BSI*.

[30] American Bureau of Shipping (ABS), 2020. Guide for fatigue assessment of offshore structures. Texas, USA.

Submitted: 29.11.2022.
Accepted: 17.01.2023.

Siri Kolle Kleivane*, Bernt Johan Leira, Sverre Steen
*siri.k.kleivane@ntnu.no
Norwegian University of Science and Technology, Department of Marine Technology, Jonsvannsveien 82, 7050 Trondheim, Norway